JOURNAL OF GEOPHYSICAL RESEARCH: ATMOSPHERES, VOL. 118, 7309–7320, doi:10.1002/jgrd.50562, 2013

Non-negligible effects of cloud vertical overlapping assumptions on longwave spectral fingerprinting studies

Xiuhong Chen,[1] Xianglei Huang,[1] and Xu Liu[2]

Received 6 February 2013; revised 2 May 2013; accepted 5 June 2013; published 10 July 2013.

[1] In order to monitor and attribute secular changes from outgoing spectral radiances, spectral fingerprints need to be constructed first. Large-scale model outputs are usually used to derive such spectral fingerprints. Different models make different assumptions on vertical overlapping of subgrid clouds. We explore the extent to which the spectral fingerprints constructed under different cloud vertical overlapping assumptions can affect such spectral fingerprinting studies. Utilizing a principal component-based radiative transfer model with high computational efficiency, we build an OSSE (Observing System Simulation Experiment) with full treatment of subgrid cloud variability to study this issue. We first show that the OLR (outgoing longwave radiation) computed from this OSSE is consistent with the OLR directly output from the parent large-scale models. We then examine the differences in spectral fingerprints due to cloud overlapping assumptions alone. Different cloud overlapping assumptions have little effect on the spectral fingerprints of temperature and humidity. However, the amplitude of the spectral fingerprints due to the same amount of cloud fraction change can differ as much as a factor of two between maximum random versus random overlap assumptions, especially for middle and low clouds. We further examine the impact of cloud overlapping assumptions on the results of linear regression of spectral differences with respect to predefined spectral fingerprints. Cloud-relevant regression coefficients are affected more by different cloud overlapping assumptions than regression coefficients of other geophysical variables. These findings highlight the challenges in constructing realistic longwave spectral fingerprints and in detecting climate change using all-sky observations.

Citation: Chen, X., X. Huang, and X. Liu (2013), Non-negligible effects of cloud vertical overlapping assumptions on longwave spectral fingerprinting studies, *J. Geophys. Res. Atmos.*, *118*, 7309–7320, doi:10.1002/jgrd.50562.

1. Introduction

[2] Recently, more attention has been paid to the methodology and feasibility of observing small, but critical, climate change signals from the spectral radiance domain over the decadal time scale [*Goody et al.*, 1998; *Goody et al.*, 2002; *National Research Council, Committee on Earth Science and Applications from Space*, 2007; *Wielicki et al*, 2013]. The Climate Absolute Radiance and Refractivity Observatory (CLARREO) mission was formulated to address past difficulties in tracking subtle climate change signals in the satellite record [*Karl et al.*, 2006]. CLARREO will enable the detection of climate change signals by benchmarking spectral fingerprints. That is, researchers will use optimal fingerprinting methods with the well-calibrated spectral radiances observed by the CLARREO to determine the changes in geophysical parameters responsible for such spectral radiance changes. The optimal fingerprinting method was proposed by *Hasselmann* [1979] and has been widely used in climate detection and attribution studies [e.g., *Hasselmann* 1993; *Venzke et al.*, 1999; *Hegerl et al.*, 2006; *Santer et al.*, 2011]. *Leroy et al.* [2006; 2008a; 2008b] have conducted many theoretical studies regarding the feasibility of benchmark spectral fingerprinting (as well as the benefit of including GPS radio occultation in such benchmark fingerprinting). In such studies, the first step is always to construct spectral fingerprints, i.e., the changes in spectral radiance caused by a change in a particular geophysical variable (or combinations of variables). Once such predefined fingerprints in the spectral domain are established, it is then possible to detect and attribute climate change signals (such as the amplitude of secular change of CO_2 and the strengths of water vapor, lapse rate, and cloud feedbacks) from the spectra. Spectral fingerprints can be constructed from geophysical parameters simulated by the general circulation model (GCM) [e.g., *Leroy et al.*, 2008b; *Huang et al.*, 2010] as well as from geophysical parameters based on observations and reanalysis [*Kato et al.*, 2011]. Meanwhile, climate observational system simulation experiments (OSSEs) play a pivotal role in CLARREO-related studies [*Feldman et al.*, 2011] and will likely be so in the planning of any future climate monitoring missions. Climate OSSEs can be built upon the GCM

[1]Department of Atmospheric, Oceanic, and Space Sciences, University of Michigan, Ann Arbor, Michigan, USA.
[2]NASA Langley Research Center, Hampton, Virginia, USA.

Corresponding author: X. Huang, Department of Atmospheric, Oceanic, and Space Sciences, University of Michigan, 2455 Hayward St., Ann Arbor, MI 48109-2143, USA. (xianglei@umich.edu)

2169-897X/13/10.1002/jgrd.50562

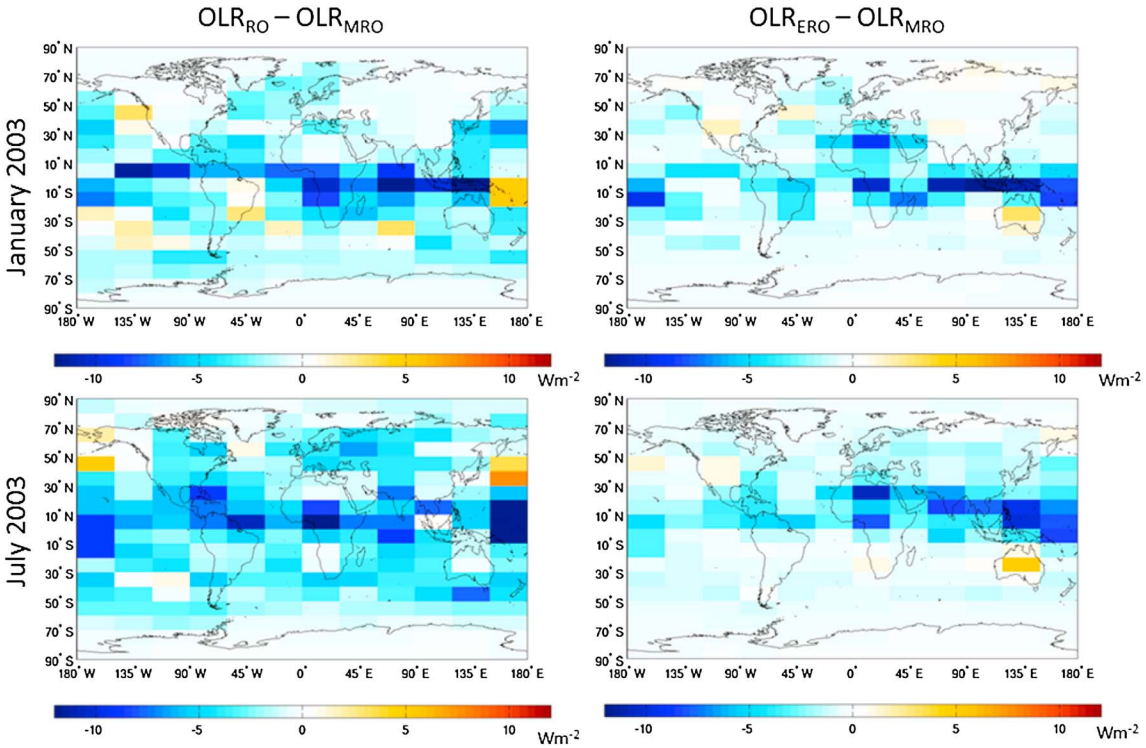

Figure 1. Maps of monthly mean differences in OLR solely due to the different cloud overlapping assumptions, i.e., the random overlap (RO) versus maximum random overlap (MRO) and the exponential random overlap (ERO) versus MRO. Global mean RO-MRO differences are -2.44 and $-3.46\,\mathrm{W\,m^{-2}}$ for 2003 January and July, respectively. The global mean ERO-MRO difference is $-1.7\,\mathrm{W\,m^{-2}}$ for both months. Results are shown for 10° latitude × 30° longitude grid boxes. Temperature, humidity, and cloud profiles are from the ECMWF ERA-interim reanalysis.

output [*Feldman et al.*, 2011], which means using GCM outputs to simulate the target variables that will be observed by the satellite over the desirable periods and exploring various questions based on such synthetic data sets of radiances.

[3] Due to the coarse spectral resolution of the GCM radiation schemes, they usually cannot be used directly to construct spectral fingerprints. A separate radiance simulator must be included in the climate OSSEs and used for this purpose. For GCM-based spectral fingerprinting and climate OSSEs, it is desirable to have the simulated radiances computed in a way that is maximally consistent with the radiation scheme of the parent GCM (including the cloud radiation scheme to compute cloud optical properties from its microphysical properties). Otherwise, it may be difficult to connect the results derived from the spectral fingerprinting and climate OSSE studies with other results and aspects of the parent GCM. For example, if a GCM cloud radiation scheme assumes that all liquid water clouds are gray bodies in the longwave but the radiance simulator assumes frequency-dependent optical properties for liquid water clouds, then the spectral fingerprint of low cloud constructed by this radiance simulator would be distinctly different from what is assumed in the parent GCM "world." Then it would be unlikely that any conclusion about low cloud feedback inferred from such spectral fingerprinting and climate OSSE studies could be consistent with the low cloud feedback in its parent GCM.

[4] When there is a need to have the spectral fingerprints derived from the radiance simulator consistent with parameterizations in the parent GCM, the following aspects need to be considered: (1) consistency in the spectroscopy of absorptive gases; (2) consistency in the calculation of cloud optical properties from cloud microphysical properties; and (3) consistency in the treatment of subgrid variability of relevant variables. The standard practice in developing any credible radiative transfer model or radiation scheme is to obtain a satisfactory benchmark performance against a state-of-the-art line-by-line radiation transfer model for the clear-sky cases. Therefore, the treatment of gaseous spectroscopy should converge and be consistent between the radiance simulator in the climate OSSE and the GCM radiation scheme at the coarse spectral resolution of the GCM radiation scheme for spectroscopic features that are significant in the troposphere. For (2), it is an issue of computer programming to ensure that the radiance simulator uses the identical cloud optical properties as the GCM cloud radiation scheme. For (3), current GCM radiation schemes usually assume no subgrid variability of temperature and humidity [e.g., *Donner et al.*, 2011; *Oleson et al.*, 2010]. Therefore, the largest contribution is from subgrid variability of clouds. Because a single cloud usually is not fully resolved at the GCM horizontal scale, cloud fraction is used in GCM radiation calculation. As a result, how to assume the vertical arrangements of multilayer clouds, usually termed as cloud vertical overlapping or simply cloud overlapping, is an important issue.

[5] Currently, two popular cloud overlapping assumptions are random overlap (hereafter, RO) [*Manabe and Strickler*, 1964] and maximum random overlap (hereafter, MRO)

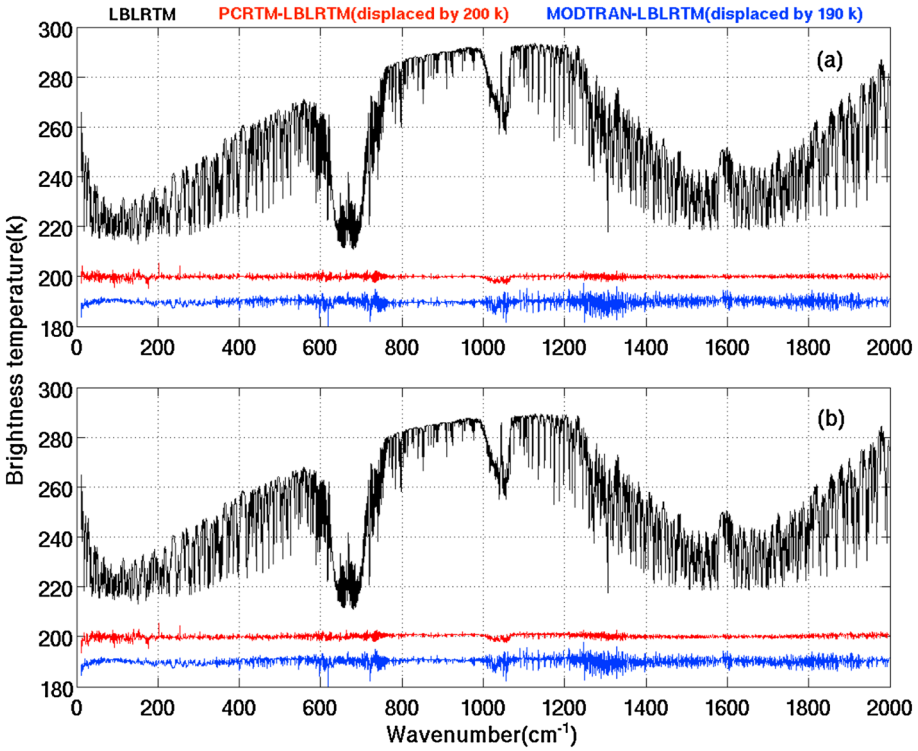

Figure 2. Comparisons between PCRTM2.1 and LBLRTM12.0 and between MODTRAN5 and LBLRTM12.0. (top) A typical tropical clear sky. (bottom) A typical overcast sky with a cirrus cloud topping at 10.2 km and of visible optical depth of 0.16. For both cases, the viewing zenith angle is 24.3°. Black lines are the spectra computed from LBLRTM 12.0. Red lines are differences between PCRTM and LBLRTM 12.0 (for better visualization, they are displaced by 200 K), and blue lines are difference between MODTRAN5 and LBLRTM 12.0 (for better visualization, they are displaced by 190 K). All spectra shown here have a spectral resolution of 1 cm^{-1} (full width at half maximum).

[*Geleyn and Hollingsworth*, 1979]. Another overlapping assumption, exponential random overlap (hereafter, ERO) [*Hogan and Illingworth*, 2003; *Pincus et al*., 2005], has also been adopted more and more by the mainstream climate modeling efforts. The ERO assumes a weighting summation of the random overlap and the maximum overlap. The weighting factor, termed as cloud overlap parameter (α), is assumed falling off exponentially with the distance between cloud layers. $\alpha = 0$ corresponds to the random overlap, while $\alpha = 1$ corresponds to the maximum overlap. *Morcrette and Jakob* [2000] studied the effects of three cloud overlapping assumptions (maximum, maximum random, and random) on cloud radiative forcing. A difference of 33.3 $W\,m^{-2}$ in top-of-atmosphere (TOA) flux was found between MRO and RO for a typical convective cloud case in the midlatitude summer. *Stephens et al*. [2004] used lidar and radar observations to examine five different cloud overlapping schemes. They compared the broadband fluxes computed from five overlapping schemes against the counterparts from the independent column approximation. They found a bias in flux up to ~10 $W\,m^{-2}$ due to overlapping schemes. *Shonk et al*. [2012] showed that the difference of shortwave and longwave cloud radiative forcing between ERO and MRO is up to 10 $W\,m^{-2}$ in marine stratocumulus regions though global difference is less than 1 $W\,m^{-2}$. As a case study, we use the 6-hourly geophysical profiles (including cloud fraction and cloud water content) from the European Centre for Medium-Range Weather Forecasts (ECMWF) ERA-interim reanalysis to compute the monthly mean TOA OLR (outgoing longwave radiation) with the RO, ERO, and MRO assumptions separately. The implementation of ERO assumes the same scale length as in the Geophysical Fluid Dynamics Laboratory climate model, the GFDL CM3 [*Donner et al*., 2011]. The radiative transfer code used in such calculations is to be described in detail in section 2. The monthly mean OLR difference between RO and MRO assumptions and between ERO and MRO assumptions are shown in Figure 1. The global difference between RO and MRO (RO-MRO) in January 2003 is −2.44 $W\,m^{-2}$, and in July 2003, it is −3.46 $W\,m^{-2}$. The global difference between ERO and MRO is −1.7 $W\,m^{-2}$ for both months. For multilayer clouds, the total cloud fraction from the RO

Table 1. Computational Cost of PCRTM, MODTRAN5, and LBLRTM[a]

Model	Number of Channels	Number of RT Calculations (N_{RT})	Averaged N_{RT} for Each Channel	Overall Time for the Computing
PCRTM	19901	964	0.048	0.05 s
MODTRAN5	19901	19901	1	6 s
LBLRTM	19901	8198549	412	224 s

[a]Identical inputs of clear-sky temperature and humidity profiles are used. Output spectral range is 10–2000 cm^{-1} with a 0.1 cm^{-1} spectral interval. A workstation with a six-core AMD Opteron CPU is used for this benchmark. RT in the table stands for radiative transfer.

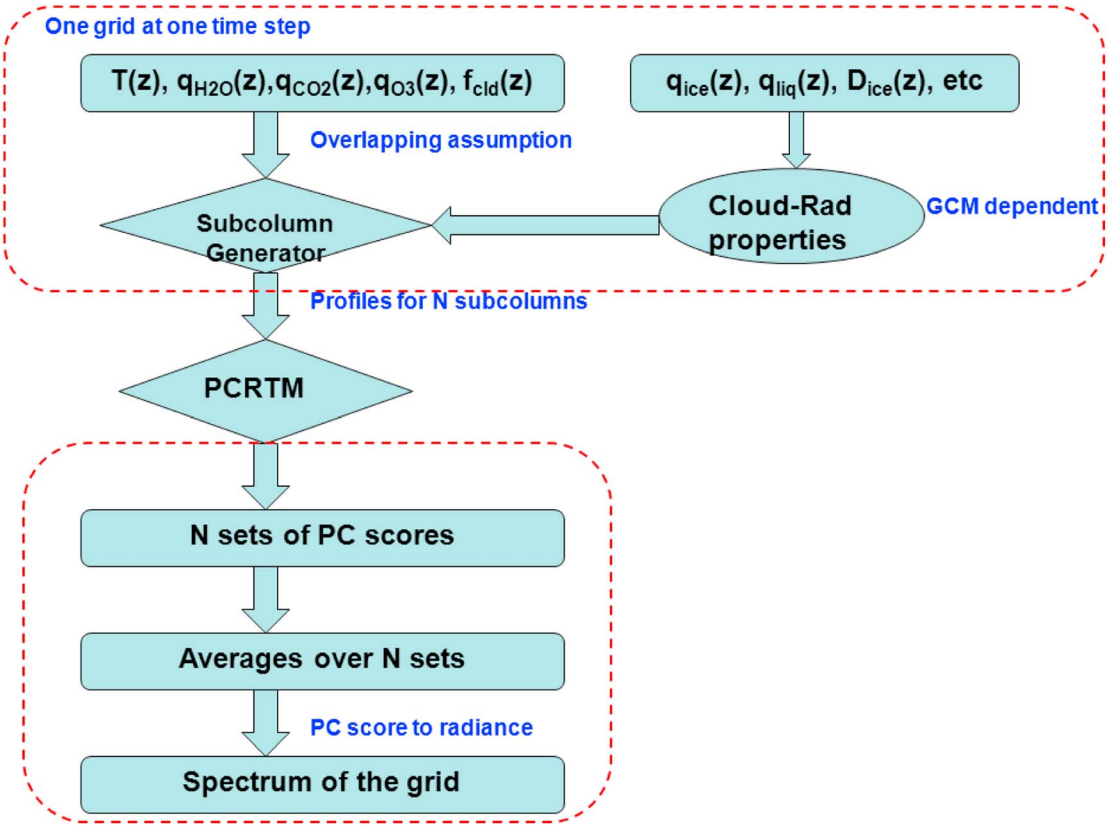

Figure 3. Flowchart summarizing the implementation of radiance simulator described in section 2. Following normal convention, T denotes air temperature, q the mixing ratio, f_{cld} the cloud fraction, and D_{ice} the effective particle size of ice clouds.

assumption is generally larger than that from the MRO assumption. Therefore, a negative RO-MRO difference as mentioned above can be expected for the global average. The RO-MRO difference over an individual grid box can be as large as $-10\,\mathrm{W\,m^{-2}}$, as is frequently seen in the tropics (Figure 1). The globally averaged ERO-MRO difference is smaller than the counterpart of RO-MRO difference, which is consistent with *Shonk et al*. [2012].

[6] Given the apparent difference that the RO and MRO assumption can lead to, it is meaningful to explore to what extent a climate OSSE and relevant fingerprinting study needs to take the cloud overlapping assumption into account. This study tries to address this question for the longwave climate OSSE and spectral fingerprints. Specifically, we examine how the RO, ERO, and MRO assumptions affect the calculations of longwave spectral radiances and, consequently, how they affect the construction of various longwave spectral fingerprints and the linear regression results using such spectral fingerprints.

[7] The rest of the paper is arranged as follows. Section 2 describes the radiance simulator and the climate OSSE that we built with full treatment of subgrid variability. It also describes the consistency between our radiance simulator output and the parent model output. The impacts of different overlapping assumptions on constructing longwave spectral fingerprints are discussed in section 3. Sections 4 and 5 present the consequential impacts on linear regression of global mean changes of all-sky spectral radiances. Conclusions and further discussions are presented in section 6.

2. A PCRTM Base Climate OSSE With Full Treatment of Subgrid Variability

2.1. PCRTM

[8] Our radiance simulator, the core of climate OSSE for spectral studies, is based on a fast and accurate thermal radiative transfer model, the PCRTM (principal component-based radiative transfer model) [*Liu et al*., 2006]. PCRTM is not a channel-based radiative transfer model; instead, it predicts the scores of precomputed principal components (PCs) in the spectral channel domain. The PC score is a nonlinear function of atmospheric state and contains essential information about the channel spectral radiances. Predefined PCs capture intrinsic channel-to-channel spectral variations, which vary little from one spectrum to another. Channel radiances are then obtained by multiplying the PC scores with prestored PCs. By computing the channel radiances in this fashion, the PCRTM achieves high accuracy and high computational efficiency [*Liu et al*., 2006]. Multiple scattering can be included in the PCRTM. To increase computational efficiency, a lookup table of reflectance and transmission of clouds is precalculated using discrete ordinates radiative transfer [*Stamnes et al*., 1988].

[9] Figure 2 shows comparisons among the spectra computed by the PCRTM 2.1, by MODTRAN5 [*Berk et al*., 2005], a radiative transfer code used in previous studies such as *Feldman et al*. [2011] and *Leroy et al*. [2008b], etc., and by LBLRTM12.0 [*Clough et al*., 2005, a benchmark

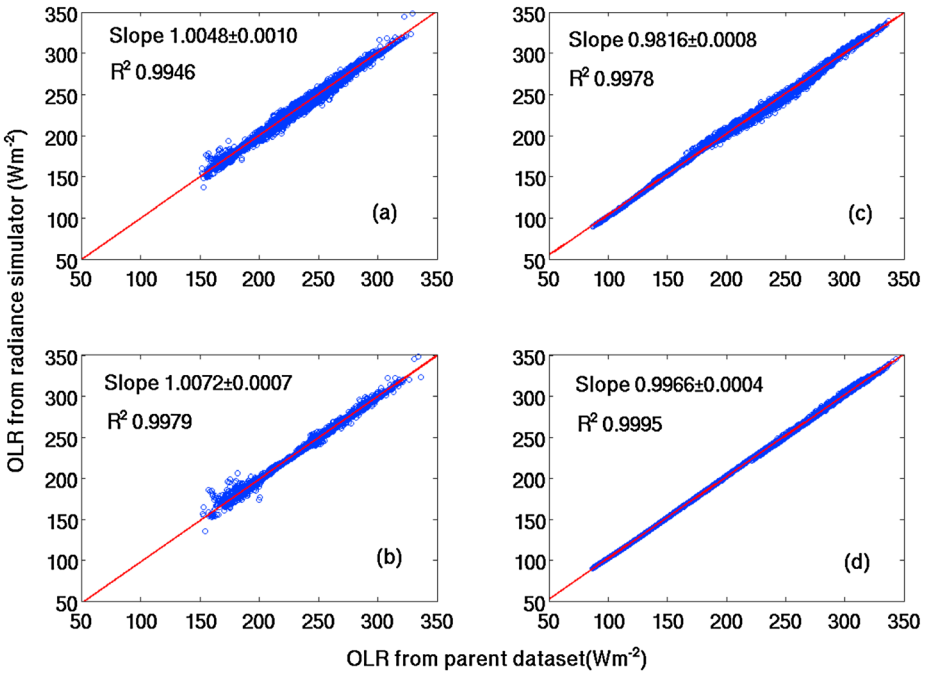

Figure 4. (a) Scatter plot of the monthly mean all-sky OLR of July 2003 in each grid box as computed from the radiance simulator and as in the ECMWF ERA-interim output over the oceans. In total results from 19,227 grid boxes are shown here. (b) Same as Figure 4a except for the clear-sky OLR in the ECMWF ERA-interim output. (c) Same as Figure 4a but based on GFDL model simulation. (d) Same as Figure 4b but based on GFDL model simulation. Slope and R-square of the linear regression are labeled on each plot.

line-by-line radiative transfer code]. All three models adopt the HITRAN2008 spectroscopic database [*Rothman et al.*, 2009]. A clear-sky profile randomly chosen from a collection of profiles used for validation of Atmospheric Infrared Sounder (AIRS) radiance simulation [*Saunders et al.*, 2007] is fed into three models to compute the TOA upward radiance. Then, an overcast profile randomly chosen in the same way as the clear-sky profile is used to do the calculation again. The root-mean-square (RMS) differences, in brightness temperature, between PCRTM and LBLRTM spectra are 0.67 K for the clear-sky case and 0.78 K for the overcast case, respectively. The RMS differences between MODTRAN5 and LBLRTM spectra are ~1.41 K for both the clear sky and the overcast sky. The computational costs of these three radiative transfer models on the same machine are listed in Table 1. MODTRAN5 is ~37 times faster than LBLRTM, while PCRTM is ~4480 times faster than LBLRTM. Thus, PCRTM is ~120 times faster than MODTRAN5, while the RMS difference of PCRTM-LBLRTM is comparable to that of MODTRAN5-LBLRTM. Note that this benchmark is for the spectral radiance output. The computational cost for PCRTM can be further reduced by half if the PC scores are the direct output instead of channel radiances. In practice, because the PC scores and PCs are linear decompositions of the spectral radiances and the precomputed PCs do not change during the computation, all linear operations (such as summation or averaging) can be done on the PC scores and only at the last step a conversion from the PC scores to the channel radiances is needed. This approach reduces the computational cost of PCRTM by half and can also save the storage cost significantly.

2.2. Implementation

[10] A chart summarizing the implementation of our OSSE is shown in Figure 3. At each grid cell and at each output time, the model archives necessary outputs of temperature, humidity, and cloud fields. To account for the subgrid variability, the grid is further divided into N subcolumns (N is predefined, and practically, it can be between 10 and 100 in our study). Then, a Monte Carlo subcolumn generator approach is used to populate clouds in all subcolumns in a way that is consistent with the cloud overlapping assumption used in the parent GCM. The details of implementing RO and MRO assumptions in such subcolumn generator can be found in *Bodas-Salcedo et al.* [2011] that described the COSP, a popular satellite simulator software package for model assessment. For exponential random overlap, the subcolumn generator follows the implementation in the GFDL CM3 cloud scheme [*Donner et al.*, 2011, and relevant references therein]. Note for each subcolumn, cloud fraction of a vertical layer is either one or zero. In parallel, cloud microphysical properties, such as ice cloud mixing ratio, liquid cloud mixing ratio, and effective size of ice cloud, are fed into a cloud radiation module so the cloud optical properties can be calculated. The cloud radiation module follows the cloud radiation scheme used in the parent GCM so a maximum consistency can be achieved between the cloud optical properties in the climate OSSE and those in the parent GCM. As a result, N sets of profiles are generated for such N subcolumns. Then PCRTM is used to compute the PC scores for each subcolumn profile. For each predefined PC component, the average over N subcolumns is the PC score for the entire grid. In our study, we find that using

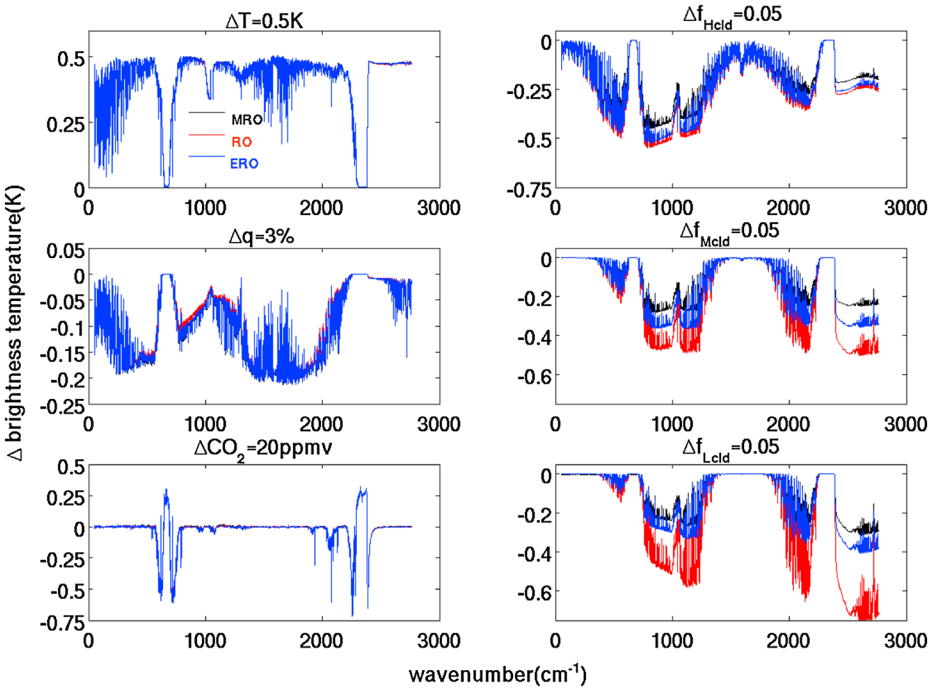

Figure 5. Spectral fingerprints derived from perturbing the 12-hourly GFDL model output in July 2003. The perturbed variable and amplitude are labeled for each panel. Results from the MRO assumption are shown in black, those from the RO assumption are in red, and those from the ERO assumption are in blue.

the first 100 PC components is accurate enough when compared to using all the PC components and the RMS difference in brightness temperature is less than 0.01 K. It is also computationally affordable to use 100 PC components even with moderate computing resources nowadays commonly available to university research groups. Thus, in our following discussions, calculations are all done using the first 100 PC components in the PCRTM calculation.

[11] This implementation has the following advantages:

[12] 1. The affordability of using subcolumn profiles makes this OSSE capable of accommodating not only the subgrid variability of clouds, but also the subgrid variability of other parameters such as temperature and humidity. One trend in current climate modeling is to have subgrid variability of humidity taken into account in PDF-based parameterization schemes [*Golaz et al*., 2002]. This OSSE will be suitable for such forthcoming improvements in GCM modeling.

[13] 2. Saving PC scores instead of the actual spectrum over each grid significantly reduces the needs for storage, which is a common issue in hyperspectral data analysis. As mentioned above, the conversion from PC scores to spectral radiances is a linear transformation so effectively, there is no need to save spectral radiances at thousands of channels for each grid box at each time step. Instead, in our study, only scores of the first 100 PC components are saved for each grid at each time step. By doing so, it requires only 1/15 of storage space for channel-based radiance simulation. If we relax, the RMS difference from the simulation of using all PCs from 0.01 to 0.1 K, the storage saving factor would be 33 since even fewer PCs are needed.

2.3. Brief Descriptions of Parent Data Sets

[14] To ensure the climate OSSE can faithfully compute spectral radiances with maximum consistency with the parent model, we use two parent data sets to test the climate OSSE separately. The GCM for one data set employs the MRO assumption, and the other employs the RO assumption. This section briefly describes the parent GCMs and data sets.

[15] The first parent data set is the 6-hourly ECMWF ERA-interim reanalysis [*Dee et al*., 2011] on 1.5° latitude by 1.5° longitude grids with 37 vertical levels in total. The ECMWF model employs RRTMG [*Mlawer and Clough*, 1997], a rapid radiation transfer model based on the correlated *k* method with maximum random overlapping assumption. Since 2007, the McICA cloud radiation scheme [*Pincus et al*., 2003] has been adopted into the RRTMG scheme used in the ECMWF model [*Morcrette et al*., 2008]. Ice cloud optical properties are derived from *Ebert and Curry* [1992], and warm cloud optical properties from *Fouquart* [1987]. ERA-interim reanalysis provides all-sky and clear-sky OLR as routine outputs. Note that the OLR is merely computed by the ECMWF model and is not an assimilated quantity. Therefore, if the climate OSSE is implemented correctly, the OLR computed by it using the ERA-interim temperature, humidity, and cloud fields should be consistent with the OLR output from the same ERA-interim reanalysis.

[16] The second parent data set is a 6-hourly output from a GFDL AM2 simulation forced by the observed sea surface temperature [*Geophysical Fluid Dynamics Laboratory Global Atmospheric Model Development Team*, 2004], which assumes the random overlap for the clouds. The horizontal resolution is 2° latitude by 2.5° longitude. It has 24 layers in vertical. The longwave radiation scheme is based on the simplified exchange approximation [*Fels and Schwarzkopf*, 1975] and is further refined in *Schwarzkopf and Ramaswamy* [1999]. Band and continuum parameters are derived from HITRAN 2000 line catalog

Table 2. Linear Regression Results When Only Temperature, Humidity, and CO_2 Mixing Ratio Are Perturbed[a]

ΔR_v^i (LHS)	ΔR_v^j (RHS)	a	b	c	R^2
MRO	MRO	0.98 ± 0.0003	1.95 ± 0.001	1.00 ± 0.001	1.00
	RO	0.97 ± 0.001	1.96 ± 0.003	1.01 ± 0.002	0.998
RO	RO	0.99 ± 0.0002	1.96 ± 0.0006	1.00 ± 0.0003	1.000
	MRO	1.00 ± 0.0006	1.95 ± 0.0023	0.99 ± 0.0011	0.999
True values		1	2	1	

[a]The definitions of $\Delta R_v^i, \Delta R_v^j, a, b, c$ can be found in section 4. R^2 is the R-square as defined in the standard linear regression statistics. Width for 95% confidence interval is also given. MRO and RO are abbreviations for maximum random overlap and random overlap, respectively. LHS (RHS) refers to the terms in the left (right)-hand side of equation (2).

[*Rothman et al.*, 2003]. Scattering is not included for the longwave radiation. Optical properties of ice clouds are derived from *Fu and Liou* [1993], and those of warm clouds are derived from *Slingo* [1989].

2.4. Validation

[17] We use the climate OSSE to compute the longwave spectral flux at TOA. The sum of such spectral flux is the OLR. The monthly mean OLR over each grid is then compared to the monthly mean OLR archived in the parent data sets. Figure 4 summarizes the comparisons between such two sets of monthly mean OLRs. For both ECMWF-interim reanalysis and GFDL AM2 model, the climate OSSE can reproduce the monthly mean OLR over each grid as computed by the parent model to a very large extent. For the four scatterplots, the linear slopes are all close to unity (0.98–1.00), and the R-squares are all larger than 99.4%. The good agreement shown in Figure 4 gives us further confidence to use this climate OSSE in the following sections.

3. Influence of Overlapping Assumptions on Spectral Fingerprint Derivation

[18] As a sensitivity study, 1 month of 12-hourly (00 UTC and 12 UTC) output from GFDL AM2 simulation in July 2003 is used to construct the spectral fingerprints. Three parallel sets of spectral fingerprints are constructed; one assuming the RO, one assuming the ERO, and the other assuming MRO assumption. Only the global mean spectrum is considered here. Six spectral fingerprints are derived: one for uniformly perturbing the tropospheric temperature by 0.5 K, one for uniformly perturbing the tropospheric humidity by 3%, one for increasing CO_2 mixing ratio by 20 ppmv, and three for changing the high, middle, and low cloud fractions by 5%, respectively. The International Satellite Cloud Climatology Project definitions of high, middle, and low clouds based on cloud top pressure (<440 hPa: high cloud; 680–440: middle cloud; >680 hPa: low cloud) are used here [*Rossow and Schiffer*, 1991].

[19] Figure 5 shows the derived spectral fingerprints for aforementioned perturbations. For temperature, humidity, and CO_2 perturbations (Figure 5, left), little difference exists between the spectral fingerprints derived with three different cloud overlapping assumptions. For the spectral fingerprint due to change of high cloud fraction, the difference between the RO and MRO assumptions is most prominent over the mid-IR (800–1200 cm^{-1} with ozone band excluded) and near-IR window (~2500–2760 cm^{-1}) regions. The difference also exists for some portions of H_2O (1200–1800 cm^{-1}) and CO_2, v_2, and v_3 fundamental bands. The centers of both CO_2 fundamental bands (667 cm^{-1} for v_2 band and 2349 cm^{-1} for v_3 band) show no difference because it saturates in the middle stratosphere and thus is insensitive to tropospheric cloud perturbations (same is true for middle and low cloud change). At all frequencies, the spectral fingerprint derived under the RO assumption has larger amplitude than that under the MRO assumption. This is consistent with what we described in section 1. The RO makes outgoing radiance sensitive to cloud fraction changes in all layers. The MRO makes the outgoing radiances less sensitive to cloud fraction

Table 3. Similar to Table 2 Except That the Cloud Fraction Is Perturbed as Well[a]

ΔR_v^i	ΔR_v^j	a	b	c	d	e	g
(LHS)	(RHS)						
				Perturbing high cloud fraction only			
MRO	MRO	0.98 ± 0.001	0.91 ± 0.002	0.98 ± 0.001	1.86 ± 0.001		
	RO	1.07 ± 0.002	1.21 ± 0.004	1.04 ± 0.002	1.57 ± 0.002		
	ERO	1.04 ± 0.002	1.12 ± 0.002	1.02 ± 0.001	1.61 ± 0.001		
True values		1	1	1	2		
				Perturbing middle cloud fraction only			
MRO	MRO	0.99 ± 0.000	0.98 ± 0.001	1.00 ± 0.000		0.99 ± 0.001	
	RO	1.08 ± 0.005	1.27 ± 0.012	1.06 ± 0.003		0.61 ± 0.004	
	ERO	1.04 ± 0.002	1.19 ± 0.004	1.03 ± 0.001		0.76 ± 0.002	
True values		1	1	1		1	
				Perturbing low cloud fraction only			
MRO	MRO	0.97 ± 0.001	0.95 ± 0.003	1.00 ± 0.001			2.03 ± 0.001
	RO	0.99 ± 0.008	1.03 ± 0.020	1.02 ± 0.005			0.88 ± 0.005
	ERO	1.00 ± 0.001	1.01 ± 0.003	1.01 ± 0.001			1.61 ± 0.001
True values		1	1	1			2

[a]For brevity, only the perturbed cases (ΔR_v^i) under the MRO assumptions are shown. The R-squares for all cases are larger than 0.99.

Table 4. Similar to Table 3 Except the Cloud Fractions of High, Middle, and Low Clouds Are Changing at the Same Time[a]

ΔR_v^i	ΔR_v^i	a	b	c	d	e	g
(LHS)	(RHS)						
				Perturbing all cloud fractions			
MRO	MRO	1.00 ± 0.001	1.04 ± 0.003	1.00 ± 0.000	1.00 ± 0.002	0.88 ± 0.005	0.65 ± 0.004
	RO	1.05 ± 0.003	1.15 ± 0.006	1.02 ± 0.002	0.92 ± 0.003	0.65 ± 0.007	0.09 ± 0.005
	ERO	1.03 ± 0.002	1.09 ± 0.005	1.01 ± 0.001	0.92 ± 0.002	0.68 ± 0.008	0.39 ± 0.007
True values		1	1	1	1	1	1

[a]For all regressions, the R-squares are larger than 0.999.

changes in the lower portion of any multilayer cloud due to the fact that the lower portion clouds are masked by the upper portion clouds as much as possible. The lower the altitude in which cloud changes occur, the more contrast between MRO and RO assumptions are likely to be seen. This explains the large differences between two sets of fingerprints for the middle cloud and low cloud perturbations, especially in the window regions. For 5% change in the high cloud fraction, the difference between the RO and MRO fingerprints in the mid-IR (800–1200 cm^{-1}) is 0.09 K in brightness temperature (Figure 5, top right). For the same change in middle and low cloud fraction, the difference becomes 0.18 and 0.24 K, respectively (Figure 5, middle and bottom). For near-IR window (2000–2760 cm^{-1}), the contrast is 0.05 K for high cloud, 0.16 K for middle cloud, and 0.27 K for low cloud changes. For middle and low cloud cases, the fingerprints are zero over vast portions of H_2O bands that saturate in the upper troposphere. Hence, there is no difference between RO and MRO cases at these spectral regions.

[20] In summary, the cloud overlapping assumptions have little impact on the spectral fingerprints of noncloud variables. As for the spectral fingerprints derived from cloud fraction changes under the RO and MRO assumptions, their spectral shapes highly resemble each other, but the amplitudes are different. The fingerprints associated with the MRO assumption always tend to have smaller amplitude due to the masking effect of upper layer cloud in such an assumption. Such differences between two assumptions are more prominent for the middle and low cloud changes than for the high cloud change. As for the cloud-related spectral fingerprints derived with the ERO assumption used in this study, their amplitudes are between those constructed with the RO and MRO assumptions. As mentioned above, the RO is at one end of the ERO with cloud overlap parameter (α) being zero, and the maximum overlap is at the other end of the ERO with α being one. The MRO, in average, is more toward the end of the maximum overlap rather than the end of the RO. Thus, it can be expected that an ERO assumption with α between zero and one results in amplitudes of cloud-related spectral fingerprints between those from the RO and MRO assumptions.

4. A Simple Linear Regression Sensitivity Study

[21] To get further insight about how different overlapping assumptions can affect the cloud changes derived using spectral fingerprinting approach, a simple linear regression study is carried out. Using the same month of GFDL AM2 output, several variables are simultaneously perturbed together, and the globally and monthly averaged spectra are computed. Then, the deviations of such spectra from the unperturbed case are calculated. Such deviations are calculated under MRO, RO, and ERO assumptions, respectively, i.e.,

$$\Delta R_v{}^i = \overline{R_v{}^i(T+\Delta T, q+\Delta q, \mathrm{CO_2}+\Delta \mathrm{CO_2}, f_{\mathrm{hcld}}+\Delta f_{\mathrm{hcld}}, f_{\mathrm{mcld}}+\Delta f_{\mathrm{mcld}}, f_{\mathrm{lcld}}+\Delta f_{\mathrm{lcld}})} - \overline{R_v{}^i(T, q, \mathrm{CO_2}, f_{\mathrm{hcld}}, f_{\mathrm{mcld}}, f_{\mathrm{lcld}})} \quad (1)$$

where the overbar represents the global and monthly average. T is temperature, q is humidity, and f is the cloud fraction with subscripts of hcld, mcld, and lcld denoting high, middle, and low cloud, respectively. The superscript i is either MRO or RO or ERO, depending on which cloud overlapping assumption used in the calculation.

Table 5a. The Regressed Coefficients for Middle Cloud Fraction Change, i.e., e in Equation (2), When Both Low Cloud and Middle Cloud Fractions Are Perturbed Under the MRO Assumptions[a]

Δf_{mcld}	Δf_{lcld}					
	1%	2%	5%	8%	10%	True value
1%	0.19 ± 0.002	0.19 ± 0.002	0.16 ± 0.003	0.10 ± 0.003	0.05 ± 0.004	0.2
2%	0.35 ± 0.003	0.37 ± 0.003	0.34 ± 0.003	0.28 ± 0.004	0.23 ± 0.004	0.4
5%	0.86 ± 0.005	0.87 ± 0.005	0.88 ± 0.005	0.84 ± 0.006	0.79 ± 0.006	1
8%	1.38 ± 0.004	1.39 ± 0.005	1.42 ± 0.005	1.41 ± 0.006	1.37 ± 0.007	1.6
10%	1.73 ± 0.004	1.74 ± 0.004	1.77 ± 0.005	1.77 ± 0.006	1.75 ± 0.007	2

[a]The spectral fingerprints under the MRO assumptions are used in the regressions. The true value of middle cloud fraction change with respect to 5% change in constructing fingerprints is also given.

Table 5b. The Ratio of Regressed Coefficients for Middle Cloud Fraction Change, e_{MRO}/e_{RO}[a]

Δf_{mcld}	Δf_{lcld}				
	1%	2%	5%	8%	10%
1%	3.21	1.96	0.79	0.35	0.15
2%	2.12	1.75	1.09	0.71	0.52
5%	1.68	1.59	1.36	1.14	1.01
8%	1.53	1.49	1.37	1.26	1.17
10%	1.48	1.45	1.36	1.28	1.22

[a]e_{MRO} is what is shown in Table 5a, while e_{RO} is regressed coefficient when fingerprints under the RO assumptions are used in the linear regression.

[22] Such differences are linearly regressed onto the spectral fingerprints constructed in section 3, namely,

$$\Delta R_v^{\,i} = a\Delta R_v^{\,j}(\Delta T_0) + b\Delta R_v^{\,j}(\Delta q_0) + c\Delta R_v^{\,j}(\Delta CO_{2_0}) + d\Delta R_v^{\,j}\left(\Delta f_{\mathrm{hcld}_0}\right) + e\Delta R_v^{\,j}\left(\Delta f_{\mathrm{mcld}_0}\right) + g\Delta R_v^{\,j}\left(\Delta f_{\mathrm{lcld}_0}\right) + r_v \quad (2)$$

[23] Where a–e and g are regression coefficients, ΔR_v^j is the spectral fingerprint constructed in section 3 with subscript 0 denoting the fixed perturbation used for deriving ΔR_v^j (in contrast to the arbitrary perturbation in equation (1)), and r_v is the residual after linear regression. Similar to the superscript i, the superscript j can be either the MRO, RO, or ERO. Note the left-hand side (LHS) of equation (2) can be obtained by assuming either the MRO, RO, ERO assumption, as with the right-hand side (RHS).

[24] A trivial case with no cloud changes using the RO and MRO assumptions is shown in Table 2. Consistent with the depiction of spectral fingerprints in section 3, regression coefficients derived using spectral fingerprints under either assumption are close enough to the true values of perturbation, regardless the ΔR_v^i being constructed with which assumptions. Similar conclusions can be reached for a range of perturbed amplitudes for temperature, humidity, and CO_2 concentration. This is easy to understand given the large similarity in spectral fingerprints of noncloud variables between the MRO and RO assumptions.

[25] When cloud fractions of high, middle, and low clouds are perturbed individually under the MRO assumption, the regression coefficients of temperature and CO_2 fingerprints derived with the MRO, RO, and ERO assumptions are still similar to each other and close to the true values (Table 3, coefficients a and c). For water vapor, the fingerprints under the MRO assumptions can lead to a regression coefficient close to the true value, while the regression using fingerprints under the RO assumptions overestimates the coefficient by 21% and 27% for the high cloud and middle cloud, respectively. Meanwhile, the regression coefficients for cloud-related fingerprints (Table 3, coefficients d, e, and g) under the RO assumption are always smaller than those under the MRO assumption. This is expected given the amplitude differences in cloud-related spectral fingerprints described in section 3. Note that, for the low cloud fraction change, the regression coefficients are different by more than a factor of two between two regressions using the RO and MRO fingerprints. In other words, if the target radiance change is from the MRO assumption, a linear regression using spectral fingerprints constructed with the RO assumption would significantly underestimate the amplitude of low cloud fraction change. Equivalently, it can be expected that if the target radiance change is from the RO assumption, a linear regression using spectral fingerprints with the MRO assumption would significantly overestimate the amplitude of low cloud fraction change.

[26] Except the regressed coefficient for temperature when only low cloud fraction perturbed (a case in which the MRO, RO, and ERO all lead to a regression coefficient close to the true value), all other regressed coefficients from the ERO assumption are bracketed by their counterparts from the MRO and RO assumptions. This fact is consistent with the relative amplitudes of spectral fingerprints with three different overlapping assumptions shown in Figure 5. These results are obtained using 5% increase of cloud fractions. Similar results can be obtained if 5% decrease of cloud fraction is used.

[27] A regression with all cloud fractions perturbed simultaneously is then carried out (Table 4). When both LHS and RHS of equation (2) are from the MRO assumption, the regressed coefficients are all close to the true values except for the low cloud fraction change, which has a regressed coefficient of 0.65 in contrast to a true value of 1. The linear fit is still satisfactory with an R-square more than 0.999. Such a good linear fit confirms that the additivity of spectral signals under such heavy averages over large spatial and temporal scales [*Huang et al*., 2010]. The large deviation of regression coefficients from the true value for the low cloud fraction change is largely due to the collinearity among different fingerprints. The correlation between middle cloud and low cloud spectral fingerprints shown in Figure 5 is 0.96, and the correlation between middle cloud and high cloud fingerprints is 0.77. Similar to the results shown in Table 3, the cloud-related regression coefficients under the MRO assumption are all larger than those under the RO assumption and than those under the ERO assumption. As expected, the largest difference in the regressed coefficients is for the low cloud fraction change (0.65 with MRO versus 0.09 with RO versus 0.39 with ERO).

Table 5c. Similar to Table 5a but for the Regressed Coefficients of Low Cloud Fraction Change, i.e., g in Equation (2)[a]

Δf_{mcld}	Δf_{lcld}				
	1%	2%	5%	8%	10%
1%	0.11 ± 0.002	0.30 ± 0.002	0.93 ± 0.002	1.58 ± 0.003	2.04 ± 0.003
2%	0.10 ± 0.002	0.25 ± 0.002	0.85 ± 0.003	1.49 ± 0.003	1.94 ± 0.004
5%	0.06 ± 0.004	0.20 ± 0.004	0.65 ± 0.004	1.24 ± 0.005	1.67 ± 0.005
8%	0.16 ± 0.004	0.28 ± 0.004	0.68 ± 0.004	1.13 ± 0.005	1.52 ± 0.005
10%	0.25 ± 0.003	0.37 ± 0.004	0.74 ± 0.004	1.16 ± 0.005	1.48 ± 0.005
True value	0.2	0.4	1	1.6	2

[a]The true value of low cloud fraction change with respect to 5% change in constructing fingerprints is also given.

Table 5d. Similar to Table 5b but for the Ratio of Regressed Low Cloud Fraction Change, g_{MRO}/g_{RO}

Δf_{mcld}	Δf_{lcld}				
	1%	2%	5%	8%	10%
1%	4.05	3.60	3.39	3.32	3.28
2%	47.80	5.63	3.75	3.51	3.42
5%	−0.91	−5.67	7.00	4.48	4.06
8%	−1.30	−3.18	28.53	7.07	5.37
10%	−1.78	−3.35	−105.37	9.90	6.91

[28] Compared to the real optimal fingerprinting studies, such a linear regression sensitivity study is highly idealized with zero natural variability and zero instrument uncertainties. Nevertheless, it shows that the cloud fingerprints constructed under different overlapping assumptions can significantly affect the regressed amplitudes of cloud changes, especially for the clouds in the lower layers. The lower the cloud is, the larger the difference in the regressed amplitude. As evident in Figure 5, fingerprints constructed under different assumptions also have slightly different spectral shapes, but such differences in the spectral shapes are secondary to the differences in the amplitude. Such amplitude difference will directly affect the estimated amplitude of changes of cloud parameters. This is likely to hold true in the presence of natural variability and instrument uncertainty as well.

5. The Impact of Different Cloud Overlapping Assumptions on Regressed Low Cloud and Middle Cloud Fraction Changes

[29] To further explore to what extent the different overlapping assumptions affect the regressed changes of low cloud and middle cloud fraction, we carry out following sensitivity study using the MRO and RO assumptions. The middle cloud fraction is perturbed with five increments, 1%, 2%, 5%, 8%, and 10%, all assuming MRO assumptions. For each middle cloud increment, the low cloud fraction is further perturbed by 1%, 2%, 5%, 8%, and 10% under the MRO assumptions, respectively. Thus, in total, there are 25 perturbed cases, and each case is regressed using equation (2) with the fingerprints from either the MRO or the RO assumptions. By doing so, the impact of MRO and RO assumptions on the regression results can further be understood when the change of low cloud fraction is different from that of middle cloud fraction.

[30] Tables 5a, 5b, 5c, 5d summarize the results regarding the regressed middle cloud fraction and low cloud fraction changes, respectively. Table 5a shows that, when both sides of equation (2) are from the MRO assumption, the regressed middle cloud fraction change is close to the true value when both the middle and low cloud fraction changes are less than 5% (the change used to construct the fingerprint). For a given middle cloud fraction change, the regressed middle cloud fraction change varies only within a small range regardless of the change of low cloud fraction (Table 5a). The only exception is the combination of 1% middle cloud change and 10% low cloud change. Similar conclusions are also true for low cloud changes when both sides of equation (2) are from the MRO assumption (Table 5c).

[31] When the perturbed low cloud fraction change is larger than the perturbed middle cloud fraction change, the regressed middle cloud fraction change under the MRO assumption (e_{MRO}) is smaller than the counterpart under the RO assumption (e_{RO}) as shown in upper right corner of Table 5b. When the perturbed low cloud fraction change is no larger than the perturbed middle cloud fraction change, the situation is just the opposite: e_{MRO} is always larger than e_{RO}. However, the ratio of e_{MRO} to e_{RO} is mostly within 0.71–1.5. This is in sharp contrast with the ratio of regressed low cloud change (Table 5d, g_{MRO} to g_{RO}), which varies from 3 to 105 in amplitude and could have a different sign. For some combinations of large changes in middle cloud fraction and small change in low cloud fraction (Table 5d, lower left corner), the ratio of g_{MRO} to g_{RO} becomes negative, i.e., regressed low cloud change is decreasing instead of increasing. For the rest of the combinations, the ratio of g_{MRO} to g_{RO} is positive and larger than 3, indicating that regressed low cloud change under the RO assumption would be smaller than the true change by at least threefold. These results further illustrate that different cloud overlapping assumptions can have a much larger impact on the regressed low cloud fraction change than the regressed middle cloud fraction change.

[32] In reality, the cloud vertical overlapping is neither strictly MRO nor strictly RO or ERO. The sensitivity studies here suggest that caution must be paid in constructing the cloud-related spectral fingerprints and in estimating the regressed amplitudes of cloud changes. The effects of cloud overlapping assumptions on these matters can be potentially large and have to be fully taken into account.

6. Conclusion and Discussion

[33] Leveraging on the computational and storage efficiency of PCRTM, we developed a climate OSSE that can take the subgrid variability of clouds into account and hence the spectral radiance can be computed in a way that is maximally consistent with parameterizations in the parent model. Using two models that employ different cloud overlapping schemes as examples, we show the consistency in simulated OLR by our OSSE and the counterparts from parent models. If needed, the subgrid variability of other variables such as temperature and humidity can be taken into account in such OSSE as well.

[34] The OSSE is then used to examine the impact of different cloud overlapping assumptions on the spectral fingerprints of cloud fraction change. The MRO, ERO, and RO assumptions mainly affect the amplitudes of the cloud-related spectral fingerprints while the impact on the spectral shape is secondary. The MRO assumption tends to have a larger masking effect for the lower-layer clouds than the RO assumption. As a result, the spectral fingerprint constructed under the MRO assumption has smaller amplitude than that under RO assumption. The difference in fingerprints for high cloud fraction change between MRO and RO assumptions is ~10–20% or even smaller while the difference for the low cloud fraction change can be much larger (Figure 5). This directly affects the regression results. While a good linear regression can be achieved for the radiance change averaged over the global and monthly timescales, the regressed coefficients for cloud fraction change can be considerably different when the fingerprints derived under different cloud overlapping assumptions are used. As shown in this simple sensitivity test, the MRO

and RO assumptions have a limited impact on the regressed high cloud fraction change and have a large impact on the regressed low cloud and middle cloud fraction changes. The most sensitive one is the low cloud fraction change, which is due to the different masking effects of different cloud overlapping assumptions as well as the collinearity between spectral fingerprints of the middle cloud and low cloud changes. As shown in Figure 5 and Tables 3, 4, the results from the ERO assumption usually lie between those from the RO and MRO assumptions. While the difficulty of using IR spectra alone to infer changes of different clouds has been pointed out before [*Huang et al*., 2010], this study indicates that the inferred cloud change is also sensitive to the cloud overlapping assumptions used in the construction of spectral fingerprints. This has not been discussed before. When it comes to applying such fingerprinting studies to real observations in the future, one practical concern is which kind of cloud overlapping assumptions should be used in constructing the spectral fingerprints. Using 1 month of CloudSat and CALIOP observations that profile three-dimensional structures of cloud fields over nearly the entire globe, *Kato et al*. [2010] showed that the scale height in the ERO assumption is not necessarily constant throughout the atmospheric column. Moreover, they showed that the scale length in such ERO assumption is physically the effective cloud geometrical thickness. Thus, with enough such three-dimensional observations of clouds, it could be possible to constrain the scale length observationally and construct cloud-related spectral fingerprints with such observationally based results.

[35] This study aims to explore the effect of different cloud overlapping assumptions in highly simplified situation with no natural variability and observational noises (instrumentation noise, sampling noise, etc.). This consists of a first step toward understanding of the impact of such assumptions in full-scale detection and attribution study using spectral optimal fingerprinting technique (which handles linear regression in the presence of natural variability and measurement noises). To take all factors into account and perform a formal spectral fingerprinting study using a decade of spectral radiances from climate, OSSE would be a follow-up study and is beyond the scope of this current study.

[36] The OSSE developed in this study in principle can be also used for data-model comparisons as well. With more than 10 years of high-quality AIRS radiances available to the public, now it is possible to evaluate long-term model simulation in the radiance domain and to examine whether model can reproduce the observed statistically significant trend seen in the AIRS spectra. To do this, instantaneous 3-hourly or 6-hourly output of simulated geophysical parameters over a decadal period would be needed (in contrast to commonly used daily mean or monthly mean output from the models).

[37] **Acknowledgments.** We wish to thank three anonymous reviewers for their constructive suggestions, which improved the clarity and readability of the paper. We are thankful to one reviewer for pointing out the importance of the ERO assumption in current modeling developments. We thank S. Klein for informative discussions on the satellite simulator in model assessment. The AM2 simulations were carried out on NOAA GFDL computing facility. The research is supported by NASA CLARREO project via NASA NNX11AE68G awarded to the University of Michigan. X.L. Huang also acknowledges the support from NASA NNX12AG66G. The ECMWF data were obtained from http://data-portal.ecmwf.int/data/d/interim_daily/.

References

Berk, A., et al. (2005), Using the MODTRAN™5 radiative transfer algorithm with NASA satellite data: AIRS and SORCE, *Proc. SPIE*, *6565*, 65651O, doi:10.1117/12.721184.

Bodas-Salcedo, A., et al. (2011), COSP: Satellite simulation software for model assessment, *Bull. Am. Meteorol. Soc.*, *92*, 1023–1043, doi:10.1175/2011BAMS2856.1.

Clough, S. A., M. W. Shephard, E. J. Mlawer, J. S. Delamere, M. J. Iacono, K. Cady-Pereira, S. Boukabara, and P. D. Brown (2005), Atmospheric radiative transfer modeling: A summary of the AER codes, *J. Quant. Spectrosc. Radiat. Transfer*, *91*, 233–244, doi:10.1016/j.qsrt2004.05.058.

Dee, D. P., et al. (2011), The ERA-Interim reanalysis configuration and performance of the data assimilation system, *Q. J. R. Meteorol. Soc.*, *137*, 553–597.

Donner, L. J., et al. (2011), The dynamical core, physical parameterizations, and basic simulation characteristics of the atmospheric component AM3 of the GFDL global coupled model CM3, *J. Clim.*, *24*, 3484–3519.

Ebert, E. E., and J. A. Curry (1992), A parametrization of ice cloud optical properties for climate models, *J. Geophys. Res.*, *97*, 3831–3836.

Feldman, D. R., C. A. Algieri, J. R. Ong, and W. D. Collins (2011), CLARREO shortwave observing system simulation experiments of the twenty-first century: Simulator design and implementation, *J. Geophys. Res.*, *116*, D10107, doi:10.1029/2010JD015350.

Fels, S. B., and M. D. Schwarzkopf (1975), The simplified exchange approximation: A new method for radiative transfer calculations, *J. Atmos. Sci.*, *32*, 1475–1488.

Fouquart, Y. (1987), Radiative transfer in climate models, in *Physically Based Modelling and Simulation of Climate and Climate Changes*, edited by M. E. Schlesinger, pp. 223–284, Kluwer Acad., Norwell, Mass.

Fu, Q., and K. N. Liou (1993), Parameterization of the radiative properties of cirrus clouds, *J. Atmos. Sci.*, *50*, 2008–2025.

Geleyn, J. F., and A. Hollingsworth (1979), An economical analytical method for the computation of the interaction between scattering and line absorption of radiation, *Contrib. Atmos. Phys.*, *52*, 1–15.

Geophysical Fluid Dynamics Laboratory Global Atmospheric Model Development Team (2004), The new GFDL global atmosphere and land model AM2-LM2: Evaluation with prescribed SST simulations, *J. Clim.*, *17*(24), 4641–4673.

Golaz, J.-C., V. E. Larson, and W. R. Cotton (2002), A PDF-based model for boundary layer clouds. Part I: Method and model description, *J. Atmos. Sci.*, *59*, 3540–3551.

Goody, R., J. Anderson, and G. North (1998), Testing climate models: An approach, *Bull. Am. Meteorol. Soc.*, *79*, 2541–2549.

Goody, R., J. Anderson, T. Karl, R. Balstad Miller, G. North, J. Simpson, G. Stephens, and W. Washington (2002), Why monitor the climate?, *Bull. Am. Meteorol. Soc.*, *83*, 873–878.

Hasselmann, K. (1979), On the signal-to-noise problem in atmospheric response studies, in *Meteorology Over the Tropical Oceans*, edited by D. B. Shaw, pp. 251–259, R. Meteorol. Soc., London.

Hasselmann, K. (1993), Optimal fingerprints for the detection of time-dependent climate change, *J. Clim.*, *6*, 1957–1971.

Hegerl, G. C., et al. (2006), Climate change detection and attribution: Beyond mean temperature signals, *J. Clim.*, *19*(20), 5058–5077.

Hogan, R. J., and A. J. Illingworth (2003), Parameterizing ice cloud inhomogeneity and the overlap of inhomogeneities using cloud radar data, *J. Atmos. Sci.*, *60*, 756–767.

Huang, Y., S. Leroy, P. J. Gero, J. Dykema, and J. Anderson (2010), Separation of longwave climate feedbacks from spectral observations, *J. Geophys. Res.*, *115*, D07104, doi:10.1029/2009JD012766.

Karl, T. R., et al. (2006), Temperature trends in the lower atmosphere: Reconciling differences, U.S. Climate Change Science Program.

Kato, S., S. Sun-Mack, W. F. Miller, F. G. Rose, Y. Chen, P. Minnis, and B. A. Wielicki (2010), Relationships among cloud occurrence frequency, overlap, and effective thickness derived from CALIPSO and CloudSat merged cloud vertical profiles, *J. Geophys. Res.*, *115*, D00H28, doi:10.1029/2009JD012277.

Kato, S., et al. (2011), Detection of atmospheric changes in spatially and temporally averaged infrared spectra observed from space, *J. Clim.*, *24*, 6392–6407.

Leroy, S., J. Anderson, and J. Dykema (2006), Testing climate models using GPS radio occultation: A sensitivity analysis, *J. Geophys. Res.*, *111*, D17105, doi:10.1029/2005JD006145.

Leroy, S., J. Anderson, and G. Ohring (2008a), Climate signal detection times and constraints on climate benchmark accuracy requirements, *J. Clim.*, *21*, 841–846.

Leroy, S., J. Anderson, J. Dykema and R. Goody (2008b), Testing climate models using thermal infrared spectra, *J. Clim.*, *21*,1863–1875.

Liu, X., W. L. Smith, D. K. Zhou, and A. Larar (2006), Principal component-based radiative transfer model for hyperspectral sensors: Theoretical concept, *Appl. Opt.*, *45*, 201–209.

Manabe, S., and R. Strickler (1964), Thermal equilibrium of the atmosphere with a convective adjustment, *J. Atmos. Sci.*, *21*, 361–385.

Mlawer, E. J., and S. A. Clough (1997), On the extension of RRTM to the shortwave region, in *Proceedings of the Sixth Atmospheric Measurement* (*ARM*) *Science Team Meeting*, *CONF-9603149,* pp. 223–226, U.S. Dep. of Energy, Washington, D. C.

Morcrette, J., and C. Jakob (2000), The response of the ECMWF model to changes in cloud overlap assumption, *Mon. Weather Rev.*, *128*,1707–1732.

Morcrette, J. J., H. W. Barker, J. N. S. Cole, M. J. Iacono, and R. Pincus (2008), Impact of a new radiation package, McRad, in the ECMWF Integrated Forecasting System, *Mon. Weather Rev.*, *136*, 4773–4798, doi:10.1175/2008mwr2363.1.

National Research Council, Committee on Earth Science and Applications from Space (2007), *Earth Science and Applications From Space*: *National Imperatives for the Next Decade and Beyond*, 456 pp., Natl. Acad. Press., Washington, D. C.

Oleson, K., et al. (2010), Technical description of version 4.0 of the Community Land Model (CLM), NCAR Tech. Note, NCAR/TN-478+STR, 257 pp., Natl. Cent. for Atmos. Res., Boulder, Colo.

Pincus, R., H. W. Barker, and J.-J. Morcrette (2003), A fast, flexible, approximate technique for computing radiative transfer in inhomogeneous cloud fields, *J. Geophys. Res.*, *108*(D13), 4376, doi:10.1029/2002JD003322.

Pincus, R., C. Hannay, S. A. Klein, K. M. Xu, and R. Hemler (2005), Overlap assumptions for assumed probability distribution function cloud schemes in large-scale models, *J. Geophys. Res.*, *110*, doi:10.1029/2004JD005100.

Rossow, W. B., and R. A. Schiffer (1991), ISCCP cloud data products, *Bull. Am. Meteorol. Soc.*, *71*, 2–20.

Rothman, L. S., et al. (2003), The HITRAN molecular spectroscopic database: Edition of 2000 including updates through 2001, *J. Quant. Spectrosc. Radiat. Transfer*, *82*, 5–44, doi:10.1016/S0022-4073(03)00146-8.

Rothman, L. S., et al. (2009), The HITRAN 2008 molecular spectroscopic database, *J. Quant. Spectrosc. Radiat. Transfer*, *110*, 533–572, doi:10.1016/j.jqsrt.2009.02.

Santer, B. D., et al. (2011), Temperature changes: The importance of timescale, *J. Geophys. Res.*, *116*, D22105, doi:10.1029/2011JD016263.

Saunders, R., et al. (2007), A comparison of radiative transfer models for simulating Atmospheric Infrared Sounder (AIRS) radiances, *J. Geophys. Res.*, *112*, D01S90, doi:10.1029/2006JD007088.

Schwarzkopf, M., and V. Ramaswamy (1999), Radiative effects of CH4, N2O, halocarbons and the foreign-broadened H2O continuum: A GCM experiment, *J. Geophys. Res.*, *104*(D8), 9467–9488, doi:10.1029/1999JD900003.

Shonk, J. K. P., R. J. Hogan, and J. Manner (2012), Impact of improved representation of horizontal and vertical cloud structure in a climate model, *Clim. Dyn.*, *38*, 2365–2376, doi:10.1007/s00382-011-1174-2.

Slingo, A. (1989), A GCM parameterization for the shortwave radiative properties of water clouds, *J. Atmos. Sci.*, *46*, 1419–1427.

Stamnes, K., S.C. Tsay, W. Wiscombe, and K. Jayaweera (1988), A numerically stable algorithm for discrete-ordinate-method radiative transfer in multiple scattering and emitting layered media, *Appl. Opt.*, *27*, 2502–2509.

Stephens, G. L., N. B. Wood, and P. M. Gabriel (2004), An assessment of the parameterization of subgrid-scale cloud effects on radiative transfer. Part I: Vertical overlap, *J. Atmos. Sci.*, *61*, 715–732.

Venzke, S., M. R. Allen, and R. T. Sutton (1999), The atmospheric response over the North Atlantic to decadal changes in sea surface temperature, *J. Clim.*, *12*, 2562–2584.

Wielicki, B. A., et al. (2013), Achieving climate change absolute accuracy in orbit, *Bull. Am. Meteorol. Soc.*, doi:10.1175/BAMS-D-12-00149.1.